J Clust Sci (2017) 28:2833–2846
DOI 10.1007/s10876-017-1262-5

ORIGINAL PAPER

Synthesis and Catalytic Activity of Alkylamine-Capped Ultra-small Palladium Nanoparticles for Organic Pollutant Degradation

K. Mallikarjuna[1] · B. Deva Prasad Raju[2] · Sumi Park[1] · Haekyoung Kim[1]

Received: 7 May 2017 / Published online: 5 July 2017

Abstract Over the past few decades, increasing attention has been focused on overcoming the scarcity of fresh water resources, with the rapid effluents of dyes from modern chemical industries causing issues in photosynthetic activity of aquatic organisms. In the process of recycling wastewater, the degradation of dye pollutants such as 4-nitrophenol, methylene blue, and methyl orange has become more crucial. Noble metal (silver, gold, palladium, and platinum) materials have significant potential applications in the areas of water purification, conversion of automobile exhaust emissions, and catalysis. Ultra-small alkylamine-capped palladium nanoparticles (APd NPs) with sizes below 10 nm are synthesized using hexadecylamine (HDA) as a stabilizing material, and HDA can prevent the irreversible aggregation of small-sized nanoparticles in solution-based reactions. The fabricated ultra-small APd NPs are investigated using UV–Vis, XRD, SEM, TEM, FTIR and TGA studies. In the presence of $NaBH_4$ as a reducing agent, the APd NPs achieve high catalytic performance toward the degradation of dye pollutants such as 4-nitrophenol, methylene blue and methyl orange.

✉ Haekyoung Kim
hkkim@ynu.ac.kr

[1] School of Materials Science and Engineering, Yeungnam University, Gyeongsan 712 749, Republic of Korea

[2] Department of Physics, Sri Venkateswara University, Tirupati 517502, India

Graphical Abstract Catalytic activity of alkylamine capped palladium nanoparticles for organic pollutant degradation.

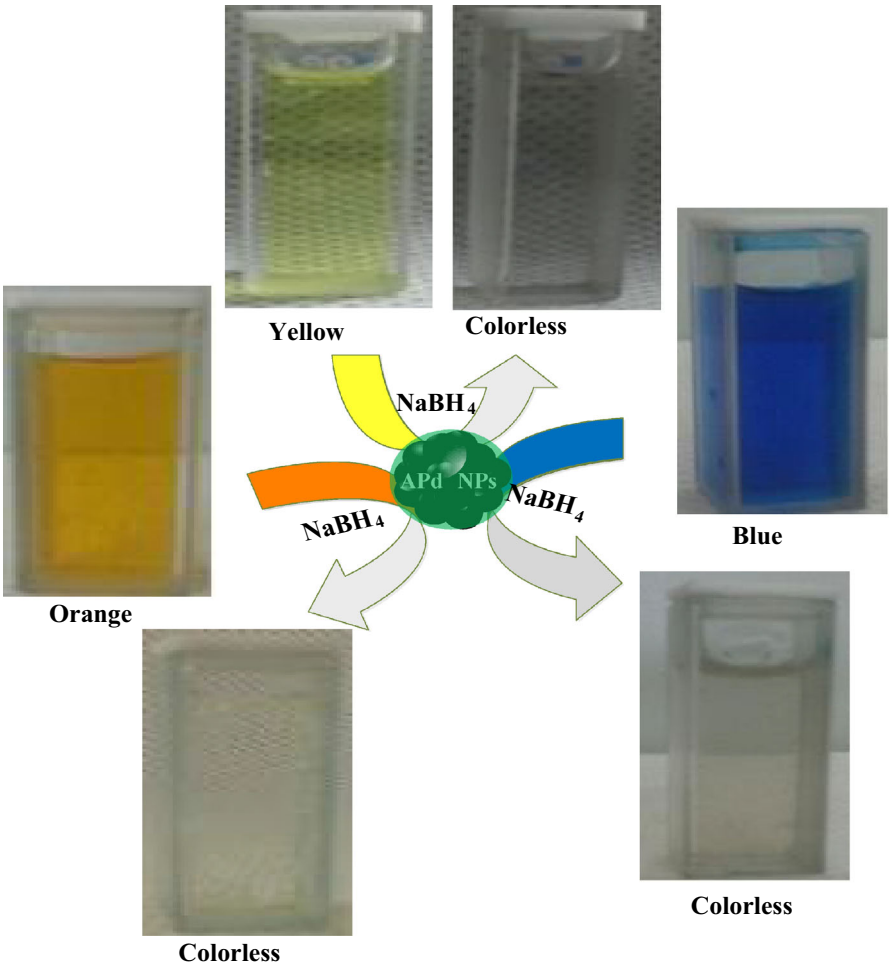

Keywords Palladium nanoparticles · Alkylamine-capped · Hexadecylamine · Catalytic activity · Organic dyes

Introduction

Recently, considering global water pollution, organic dyes are the foremost group of pollutants in wastewater discharged from different industries, such as the textile, paper, paints, printing, cosmetic, food, pharmaceutical, and pulp industries [1–3]. The reduction/adsorption or removal of organic dyes in wastewater is a demanding task because these dyes cause skin irritation, coughing, eye irritation, dyspnea,

ulcers, lung disease, sore and painful nipples, respiratory inhibition, and several cancers [4, 5]. Due to the scarcity of surface and ground freshwater resources, the reduction of organic pollutants in wastewater has become more crucial. Consequently, organic pollutants have to be removed from the water using a suitable sanitization method. International standard purification methods, such as chemical precipitation, photo-catalysis, membrane systems, biological treatment, coagulation, and adsorption onto organic and inorganic materials have been developed to remove organic pollutants [6–11]. Hence, the catalytic treatment of metal (silver, gold, palladium and platinum) nanoparticles has recently garnered increasing attention in the degradation of pollutants for environmental remediation [12]. Recently, research on metal-based materials in catalysis at the nano-scale level has received significant consideration due to their novel optical, catalytic, sensing and electrochemical properties. These properties can be tuned through controlling their shapes, sizes and morphologies at the nano-scale [13–15]. Among the metals, palladium is a multipurpose material that has various potential applications in many fields. In industrial and automotive fields, the palladium-based materials are widely used due to its ability to absorb hydrogen due to the structural changes involved in hydrogenations [16], oxidations [17], reduction [18], imaging [19], drug delivery [20], cancer diagnosis [21], carbon–carbon coupling [22] and electrochemical reactions [23–25]. Thus the synthesis of nano-sized noble metal nanoparticles is a very active investigation area because these objects may exhibit superior properties derived from their high surface to volume ratio and quantum confinement effects [26]. However, nanoparticles with small sizes under reaction conditions tend to aggregate and lose their catalytic activities due to instability and they are susceptible to irreversible aggregation in the liquid phase due to their high surface energy, which results from the high surface-to-volume ratio [27]. In order to overcome the abovementioned issues, the immobilizing nanoparticles with a specific morphology on various supports of polymers, carbon materials, dendrites, and long alkyl chains could be an efficient approach between a catalyst and its supported medium [28–31]. Moreover, the industrial applications of these nanoparticles are also hindered because they are their expensive and have limited resources. The synthesis of alkyl-amine capped nanoparticles was synthesized with alkylamine materials such as HDA, octadecylamine (ODA) and oleylamine (OA) [32–35]. Nonetheless, alkylamines are weak reducing agents that cannot reduce metal ions at <110 °C [36]. To overcome this problem, in order to attain an additional reducing agent is a key factor which should be carefully considered and chosen besides the solvent and the capping material [37]. When we design an aqueous synthetic system for ultra-small nanocrystals, it is essential for the selection of an appropriate reducing agent.

Therefore, in this research, alkylamine-capped palladium nanoparticles with high surface area is synthesize to prevent irreversible aggregation and investigated as a catalyst for the reduction of organic dyes in aqueous media. The advantage of alkyl chain protection for nanoparticles enhances their catalytic performance in the reduction of dye pollutants such as 4-nitrophenol, methylene blue and methyl orange reductions. In this approach, glucose was used as an external reducing agent for the alkylamine functionalized synthesis of ultra-small nanoparticles, which endured the use temperature lower than 110 °C.

Experimental

4-Nitrophenol (4-NP, $C_6H_5NO_3$), methylene blue (MB, $C_{16}H_{18}N_3ClS$), methyl orange (MO, $C_{14}H_{14}N_3NaO_3S$), sodium borohydride ($NaBH_4$), HCl, isopropanol and hexane were purchased from Acros Organics (USA). Palladium chloride ($PdCl_2$), hexadecylamine ($C_{16}H_{35}N$) and glucose ($C_6H_{12}O_6$) were obtained from Sigma-Aldrich (USA). All chemicals were used without further purification. Deionized water was used throughout the experimental process.

The optical properties of the prepared nanoparticles were investigated using with a UV–Vis spectrophotometer (Thermo Scientific Genesys10S, USA) with a resolution of 1 nm. X-ray diffraction (XRD) analysis to characterize the crystallography, a thin film APd NP solution was prepared using a drop casting method. The Bragg's diffraction peaks of the prepared thin film were obtained using PANalytical X'Pert PRO diffractometer equipped with a position sensitive detector, and the data were collected using Cu-Kα_1 radiation of 1.54 Å. The morphology of the APd NPs was determined using an electron microscope (SEM, S4800 Hitachi model, TEM, FEI Tecnai G2 F20). Alkylamine-capped Pd NPs were used to characterize the surface morphology, size and distribution of the nanoparticles, which were prepared through dropping the suspension onto a substrate and allowing the solvent to completely evaporate. From Fourier transform infrared (FTIR) analyses, the functional groups of HDA and APd NPs were analyzed with a JASCOFTIR spectrophotometer operated at a resolution of 4 cm^{-1} in the range of the 4000–700 cm^{-1}. The Thermo gravimetric (TG) analysis of alkylamine capped Pd NPs was analyzed up to 800 °C in N_2 at heating rate 10 °C/min with the SDT Q600 model TA instruments.

The aqueous synthesis of the APd NPs included 0.015 M of $PdCl_2$ as a precursor of Pd, 0.030 M of glucose as a reductant, and 0.060 M of hexadecylamine (HDA) as the encapsulated material. First, the 20 ml of $PdCl_2$ aqueous solution was prepared with 4% HCl. Glucose, HDA, and aqueous $PdCl_2$ were placed in a glass vial, and the mixer solution was magnetically stirred at room temperature. Then, the glass vial was sealed with paraffin tape, placed in an oven, and heated at 100 °C for 6 h. During the reaction process, the solution changed color from yellow to black.

The catalytic activity of the models for the reduction of organic dyes, such as methylene blue, methyl orange, and 4-nitrophenol, in the presence of $NaBH_4$ was analyzed using a standard quartz cuvette with a 10 mm path length, and these were investigated using a UV–vis spectrometer in order to observe the catalytic activity of the APd NPs in an ambient condition. Aqueous solutions of 4-NP (10 mM), APd NPs (1 mg/2 mL), and $NaBH_4$ (10 mM) were prepared with DI water. In order to measure an appropriate solution of 3 ml $NaBH_4$, 50 μL of 4-NP was added to a standard quartz cuvette, and the light yellow color of the 4-nitrophenol changed to dark yellow due to the formation of 4-nitrophenolate ions. Furthermore, after adding an appropriate amount of APd NP stock solution, the solution underwent UV–Vis absorption studies. The time-dependent absorbance spectra were measured at different time intervals in the scanning range of the UV–visible region. A similar

procedure was followed in order to investigate the catalytic activity of methylene blue and methyl orange.

Results and Discussion

During the synthesis, the amphiphilic fragments of HDA containing alkyl chains with a $–NH_2$ group and a non-polar $–(CH_2)_{15}–CH_3$ alkyl chain created various anisotropic structures such as flowers, nanotriangles, nanowires, rods, cubes and tadpole-like structures [38]. In this connection, the NH_2 group of HDA was adsorbed onto the surface of the palladium nanoparticles in the aqueous medium. The growth process of the alkylamine-capped palladium nanoparticles is presented in Scheme 1. The polar group of amines allowed binding onto the surface of the palladium nanoparticles in the aqueous solution, and the alkyl chain bound preferentially to the side facets of the Pd NPs, which could cause the preferential growth toward the axial (100) facets [39].

UV–Vis Absorption Studies

The reduction of the palladium chloride ions in the aqueous medium was analyzed through UV–Vis spectroscopy (Fig. 1), which exhibited the formation of APd NPs after the complete reduction of the Pd ions in the aqueous medium. The formation of APd NPs was confirmed through the disappearance of the absorbance band at 470 nm for the aqueous palladium precursor solution, which is robust evidence of the reduction of the ionic state of palladium and the formation of palladium nanostructures.

Microscopic and Structural Studies

The size, shape, and morphology of the APd NPs were investigated using transmission electron microscopy (TEM) and scanning electron microscopy (SEM) images as depicted in Figs. 2 and 3. From these images, it can be observed that the nanoparticles had a cluster of various shape including spherical, sheet, and wrinkled polyhedrons. These clusters consist of very small sized particles, with most particles

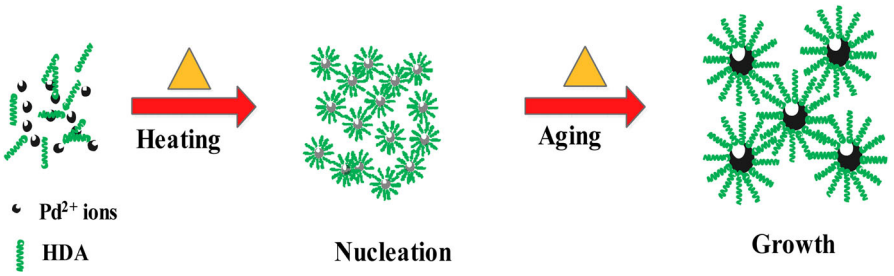

Scheme 1 Schematic diagram of formation of alkylamine capped palladium nanoparticles

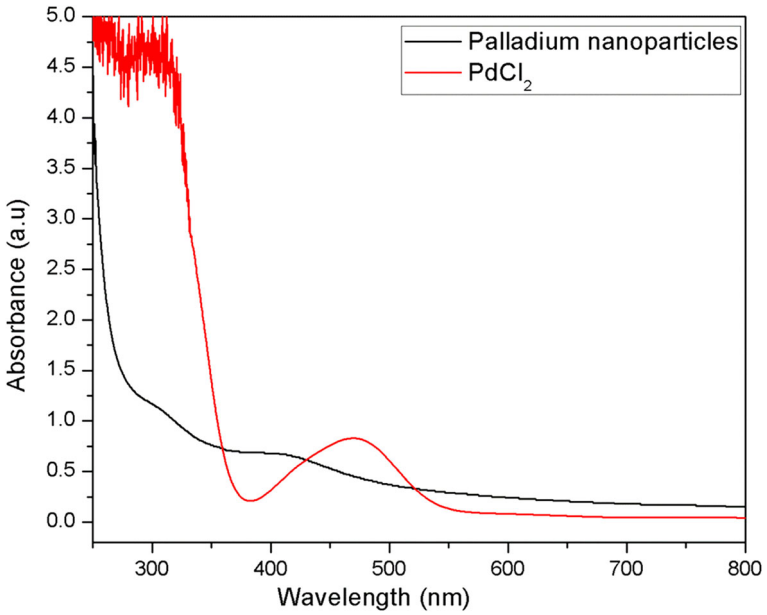

Fig. 1 UV–Vis absorption spectrum of palladium chloride and palladium nanoparticles

having diameters of 2–10 nm (Fig. 3). The ultra-fine nanoparticles had high catalytic behavior, which can be used for industrial and environmental processes such as pollutant oxidation in exhaust catalytic converters [40]. However, considering the structure, the surface could be considered not precisely spherical in shape: there were surfaces that indicated polyhedron-shaped particles. The deviation from the spherical geometry to a faceted morphology resulted from the surface energy minimization process. Hence, the whole lattice was pressed and the atoms occupied the smallest thermodynamically favorable energy positions. In the face centered cubic (FCC) lattice, the (111) facet had the lowest surface energy compared with the (100) and (110) planes. Hence, the surface atoms had a strong tendency to occupy (111) compatible positions. It is believed that the palladium nanoparticles with larger sizes were formed due to the Ostwald ripening process [41, 42]. The crystalline nature of the APd NPs was analyzed using Bragg's XRD patterns, as depicted in Fig. 4. The Bragg's diffracted peak positions were observed at 40.1°, 46.6°, 68.0°, and 82.0° which correspond to the (111), (200), (220), and (311) facets of the FCC lattice of palladium. The lattice constant (3.88 Å) and inter-planar arrangement ($d_{h\ k\ l}$) values (2.24, 1.94, 1.37, and 1.17 Å), which were calculated from the XRD spectrum of the APd NPs, were in good agreement with the standard palladium values (JCPDS File:00-005-0681 PDF file).

FTIR Analysis

FTIR spectroscopy is a valuable tool for understanding the role of HDA in the formation of Pd NPs and for investigating the chemical surroundings on the surface

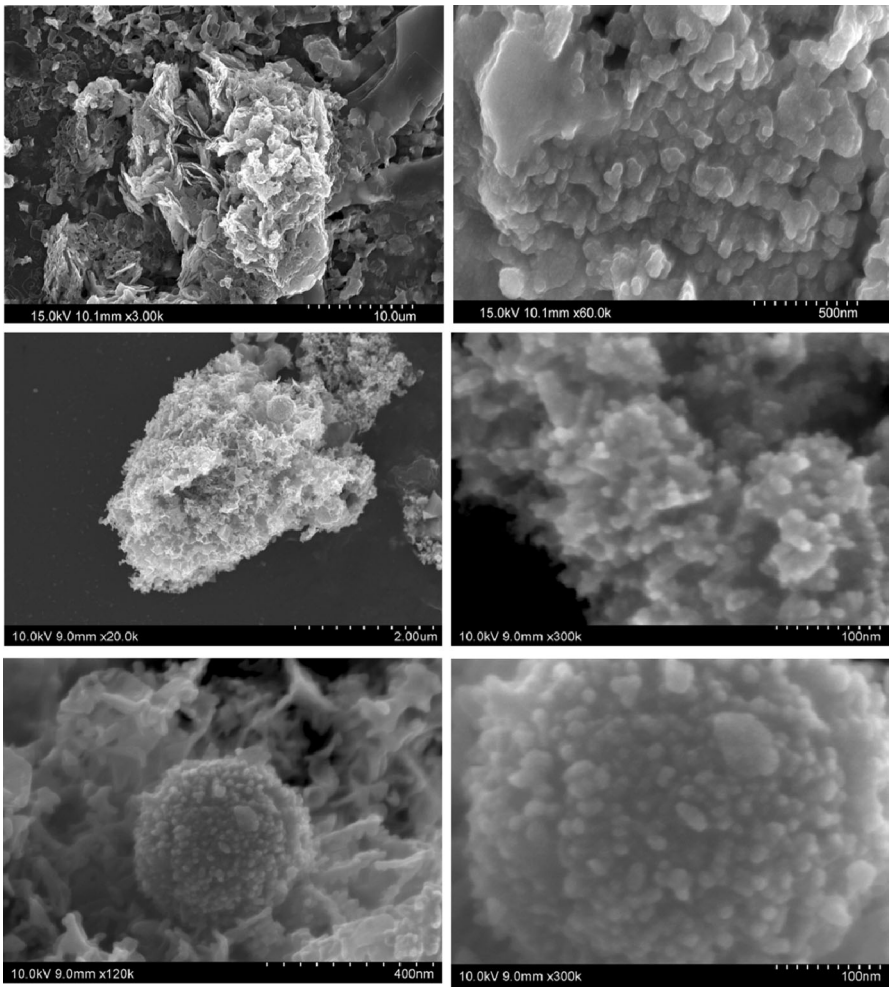

Fig. 2 SEM images of alkylamine capped palladium nanoparticles

of the Pd NPs (Fig. 5). It was revealed that, both HDA and APd NPs exhibited similar spectra, which indicates that HDA was part of the adsorbed layer of nanoparticles. The peaks of the symmetrical (3331 cm^{-1}), asymmetrical stretching vibration (3165 cm^{-1}), and overtone (3265 cm^{-1}) resulted from the N–H stretching vibration mode of the free HDA. For the APd NPs, there was a blue shift of approximately $\sim$30 cm^{-1}, associated with the binding of the amine group of the HDA adsorption of the palladium nanoparticles surface [43]. The vibration modes at 2917 and 2847 cm^{-1} were respectively attributed to the symmetric and asymmetric C-H stretching terminal modes of the CH_3 and CH_2 group alkyl chains of HDA [44]. The peak at 1607 cm^{-1} was associated with the N–H bending mode vibrations, and the modes at 1462 and 1362 cm^{-1} were assigned to the C-H bending vibration of CH_3 and CH_2, respectively: these modes shifted slightly to 1585, 1362, and

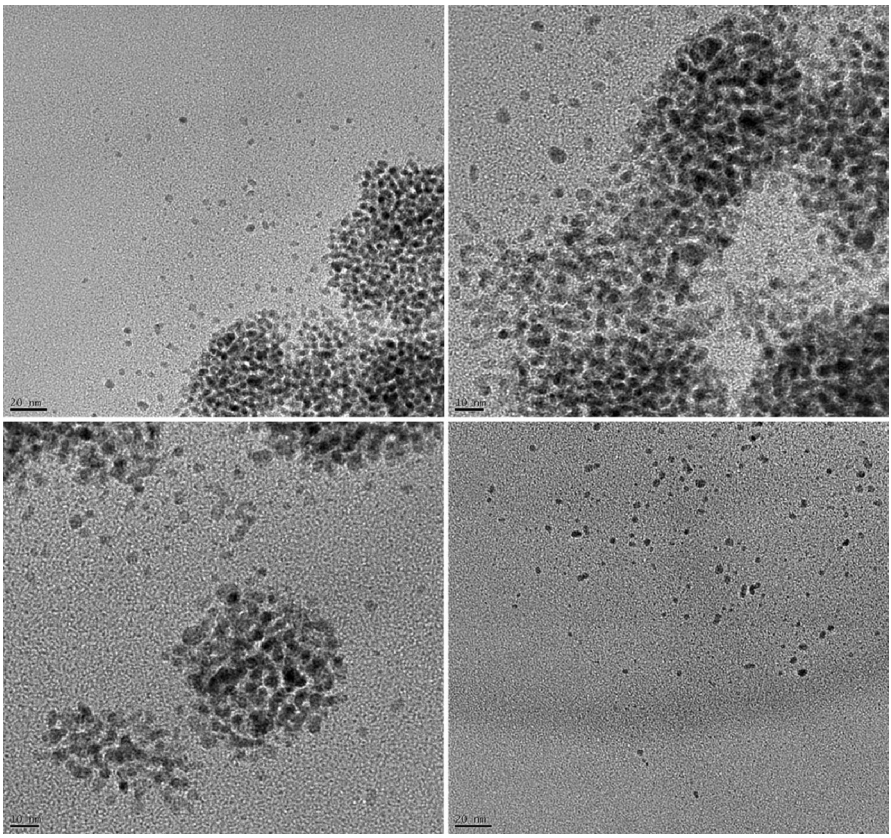

Fig. 3 TEM images of alkylamine capped palladium nanoparticles

1372 cm^{-1} [45]. The shifting of these modes indicates that the organic moieties are part of the nanoparticle synthesis. In addition, the difference in the intensity of the peaks denotes that the alkylamine molecules were present on the surface of the nanoparticles, which provided a relatively closely packed HDA layer constrained by the molecular motion, which is related to the difference in the intensities of the spectra.

TG Analysis

The thermo gravimetric analysis is a valuable analytical technique to determine the organic weight fraction of ligand stabilized metal NPs and to study the thermal stability of metal NPs at higher temperatures. From Fig. 6, the thermal decomposition of surface layer HDA (C_{16}–NH_2) on Pd NPs was studied at higher temperature region 20–800 °C. The initial 5% weight loss between 20 and 220 °C was attributed to loss of the bound solvent molecules and dissociation of the instable organic molecules in the alkylamine capped Pd NPs. Further the second step 220–500 °C, 69% weight loss was due to the consequence of the thermal

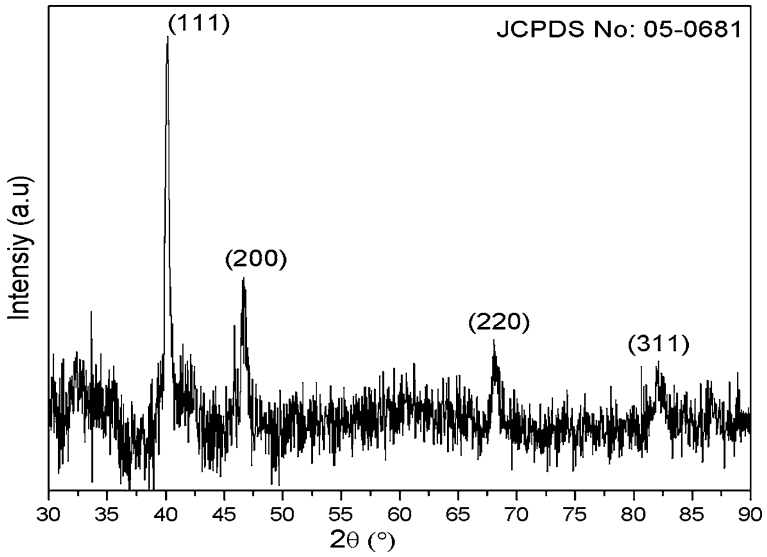

Fig. 4 XRD spectrum of alkylamine capped palladium nanoparticles

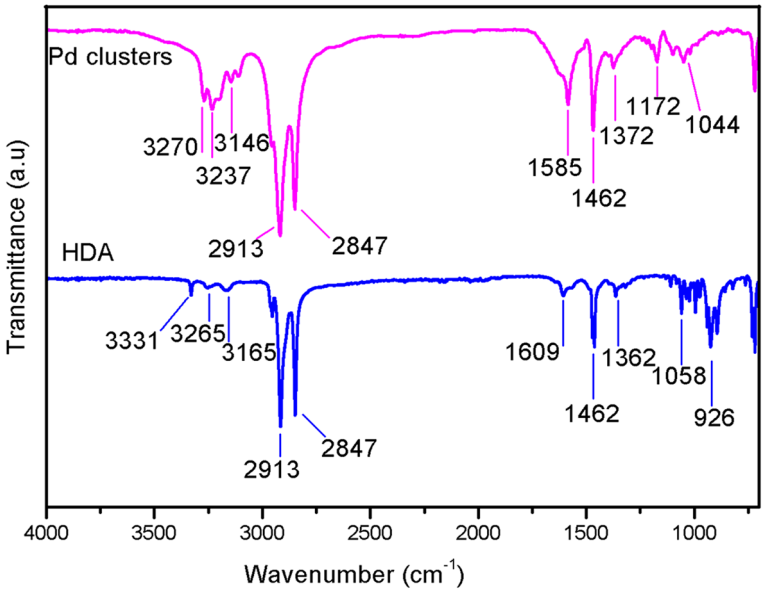

Fig. 5 FTIR spectra of Hexadecylamine (HDA) and APd NPs

degradation of organic molecules of alkylamine (HDA) which are wrapping around the Pd NPs, normally metal particles in ultra-small size have larger organic mass fractions [46]. While in third step 500–800 °C, 25.8 wt% was obtained for the residue, which mainly consisted of palladium. The residue's wt% is close to the

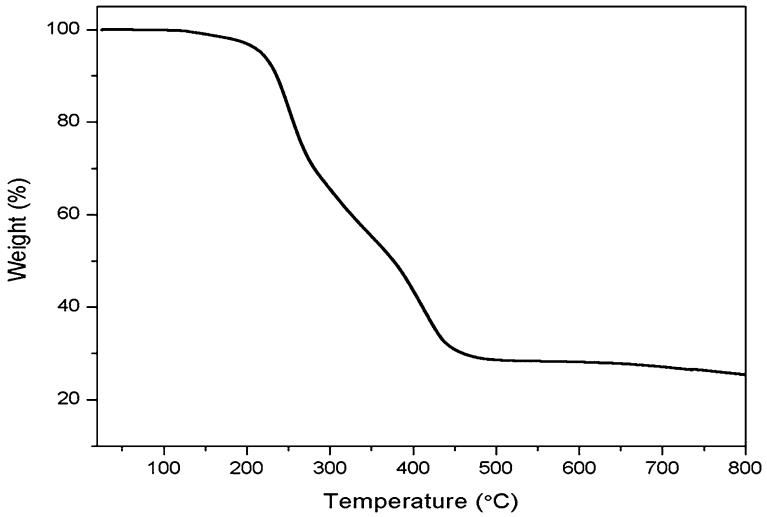

Fig. 6 Thermo gravimetric analysis of alkylamine capped Pd NPs

wt% of Pd in APd NPs. Hence, the results suggest that HDA is the main capping ligand material on Pd NPs.

Catalytic Studies

The catalytic performance of the APd NPs was investigated using organic dyes of 4-nitrophenol, methylene blue, and methyl orange with $NaBH_4$ in the aqueous medium. The continuous reduction kinetics of 4-nitrophenol, methylene blue, and methyl orange were followed by the UV–Vis absorption spectroscopic analysis. When the 4-NP was added to $NaBH_4$, the color of 4-NP changed from pale yellow to dark yellow. This was monitored by an absorption peak at 400 nm in the UV–Vis spectrum due to the formation of the 4-nitrophenolate anion (Fig. 7a). With the addition of the APd NPs, there was a significant decrease in the intensity of the absorption peak at 400 nm, and two new peaks at 300 and 230 nm emerged simultaneously due to the formation of 4-aminophenol presented in Fig. 7b [47]. The reduction kinetics of the 4-nitrophenol with presence/absence of catalyst is shown in Fig. 7c. When MB was added to $NaBH_4$, the solution changed to a light blue color and produced an absorption band at 664 nm in the UV–Vis spectrum, as depicted in Fig. 7d. After the addition of the APd NPs, there was a significant decrease in the intensity of the absorption peak at 664 nm represented in Fig. 7e and reduction kinetics of the methylene blue with before/after addition of

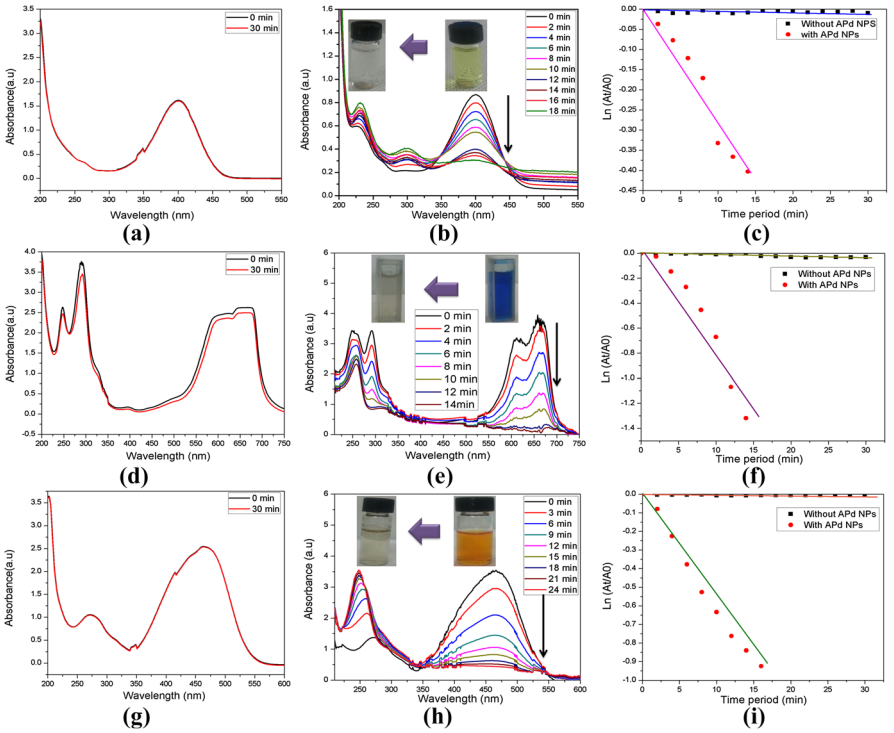

Fig. 7 UV–Vis absorption spectra of **a** without APd NPs, **b** with APd NPs, **c** kinetics of degradation of 4-nitrophenol, **d** without APd NPs, **e** with APd NPs, **f** reduction kinetics of methylene blue, **g** Without APd NPs, **h** with APd NPs and **i** kinetics of degradation of methyl orange

catalyst is exhibited in Fig. 7f [48]. With the addition of methyl orange to $NaBH_4$ the solution changed to a light orange color and produced an absorption band at 466 nm in the UV–Vis spectrum [49], as depicted in Fig. 7g. Subsequently, with the addition of the APd NPs, there was a notable decrease in the intensity of the absorption peak at 466 nm (Fig. 7h). The results revealed that the APd NPs successfully catalyzed the reduction reaction, which was almost complete within 20 min in the presence of $NaBH_4$. The reduction kinetics of the methyl orange with/without presence of catalyst is presented in Fig. 7i. In the catalytic behavior of the APd NPs, the nanoparticles functioned as electron exchangers: they took takes electrons from BH_4^- and transferred the electrons to the organic dye through functioning as a redox catalyst, which exhibited an electron relay effect. The potential reduction mechanism of the organic dyes with $NaBH_4$ in presence of the APd NPs as represented in Scheme 2. The alkyl chain of the capping material can be lengthy, and the particles are very active catalytic agents, provided that the particles are stable and the stabilizer is physio-chemically coordinated to the nanoparticle surface.

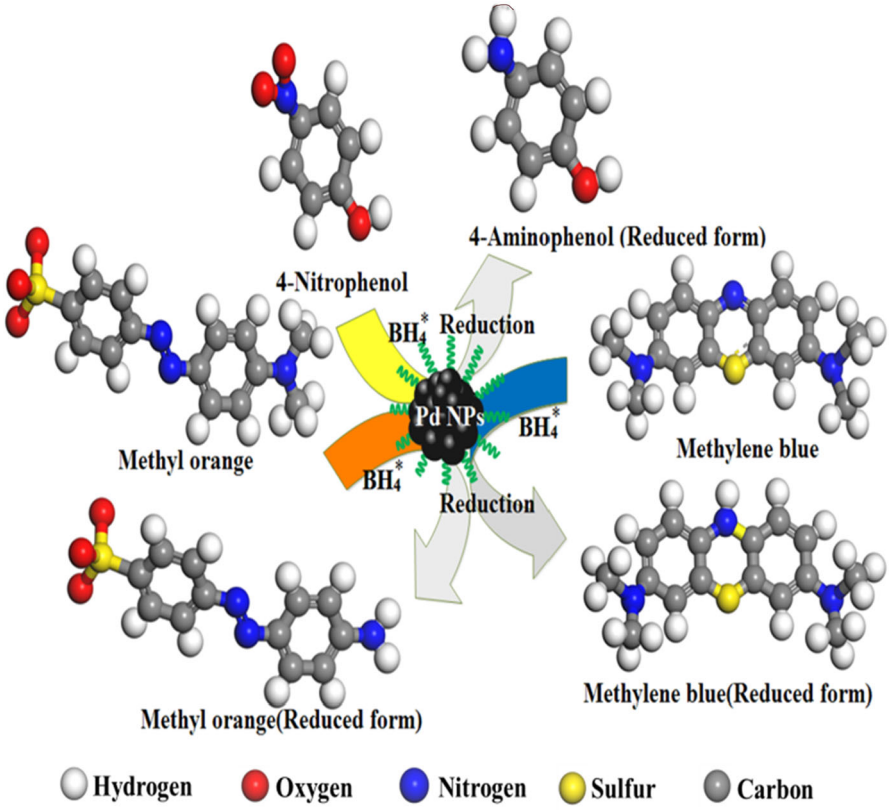

Scheme 2 The reduction mechanism of 4-nitrophenol, methylene blue, methyl orange and their reduced forms in the presence of $NaBH_4$ with APd NPs

Conclusion

In summary, an aqueous-based system was developed for the synthesis of Pd NPs (below 10 nm) stabilized with alkylamine surfactants. In this approach, glucose was used as an external reducing agent for the alkylamine functionalized ultra-small nanoparticles, which endured the use temperature lower than 110 °C. The synthesized APd NPs had excellent catalytic properties and can be used in the degradation of different organic dyes such as 4-nitrophenol, methylene blue and methyl orange using $NaBH_4$.

Acknowledgements This work was supported by the 2016 Yeungnam University Research Grant.

References

1. H. Zollinger *Colour Chemistry Synthesis, Properties and Applications of Organic Dyes and Pigments* (VCH, New York, 1987), pp. 92–102.
2. A. Bafana, S. S. Devi, and T. Chakrabarti (2011). *Environ. Rev.* **19**, 350.

3. R. E. Kirk and D. F. Othmer *Encyclopedia of Chemical Technology*, vol. 7, 5th ed (Wiley-Interscience, New York, 2004).
4. S. Vanhulle, M. Trovaslet, E. Enaud, M. Lucas, S. Taghavi, D. van der Lelie, B. van Aken, M. Foret, R. C. A. Onderwater, D. Wesenberg, S. N. Agathos, Y. J. Schneider, and A. M. Corbisier (2008). *Environ. Sci. Technol.* **42**, 584.
5. L. Pereira and M. Alves *Dyes-Environmental Impact and Remediation, Environmental Protection Strategies for Sustainable Development* (Springer Science, Berlin, 2012), pp. 111–162.
6. L. Soler and S. Sánchez (2014). *Nanoscale* **6**, 7175.
7. D. Parasuraman and M. J. Serpe (2011). *ACS Appl. Mater. Interfaces* **3**, 2732–2737.
8. H. Lachheb, E. Puzenat, A. Houas, M. Ksibi, E. Elaloui, C. Guillard, and J. M. Herrmann (2002). *Appl. Catal. B* **39**, 75.
9. M. Ahmad, E. Ahmed, Z. L. Hong, W. Ahmed, A. Elhissi, and N. R. Khalid (2014). *Ultrason. Sonochem.* **21**, 761.
10. L. Zhou, O. González, A. Carmen, S. Mazon, L. Chen, H. Deng, and M. Sui (2016). *Catal. Sci. Technol.* **6**, 5972.
11. M. S. Khehra, H. S. Saini, D. K. Sharma, B. S. Chadha, and S. S. Chimni (2005). *Water Res.* **39**, 5135.
12. X. Liu, J. Iocozzia, Y. Wang, X. Cui, Y. Chen, S. Zhao, Z. Li, and Z. Lin (2017). *Energy Environ. Sci.* **10**, 402–434.
13. A. Chen and C. Ostrom (2015). *Chem. Rev.* **115**, 11999.
14. C. N. R. Rao, G. U. Kulkarni, P. J. Thomas, and P. P. Edwards (2000). *Chem. Soc. Rev.* **29**, 27.
15. M. L. Brongersma and V. M. Shalaev (2010). *Science* **328**, 440.
16. K. Jerabek (1989). *J. Mol. Catal.* **55**, 244.
17. W. Wu and H. Jiang (2012). *Acc. Chem. Res.* **45**, 1736.
18. J. R. Prakash, A. H. McDaniel, M. Horn, L. Pilione, P. Sunal, R. Messier, R. T. McGrath, and F. K. Schweighardt (2007). *Sens. Actuators B* **120**, 439.
19. T. M. Liu, J. Conde, T. Lipiński, A. Bednarkiewicz, and C. C. Huang (2016). *NPG Asia Mater.* **8**, e295.
20. K. Shanthi, K. Vimala, D. Gopi, and S. Kannan (2015). *RSC Adv.* **5**, 44998.
21. J. W. Xiao, S. X. Fan, F. Wang, L. D. Sun, X. Y. Zheng, and C. H. Yan (2014). *Nanoscale* **6**, 4345.
22. G. B. B. Varadwaj, S. Rana, and K. Parida (2014). *J. Phys. Chem. C* **118**, 1640.
23. K. N. Mahesh, R. Balaji, and K. S. Dhathathreyan (2016). *Int. J. Hydrogen Energy* **41**, 46.
24. S. Banerjee, G. M. Narasimhaiah, A. Mukhopadhyay, and A. Bhattacharya (2016). *J. Phys. Chem. C* **120**, 25806.
25. H. Bahruji, M. Bowker, G. Hutchings, N. Dimitratos, P. Wells, E. Gibson, W. Jones, C. Brookes, D. Morgan, and G. Lalev (2016). *J. Catal.* **343**, 133.
26. B. R. Cuenya (2010). *Thin Solid Films* **518**, 3127.
27. B. C. Gates (1995). *Chem. Rev.* **95**, 511.
28. K. Karami, M. Ghasemi, and N. H. Naeini (2013). *Catal. Commun.* **38**, 10.
29. G. Prieto, J. Zečević, H. Friedrich, K. P. de Jong, and P. E. de Jongh (2013). *Nat. Mater.* **12**, 34.
30. M. Moreno, L. N. Kissell, J. B. Jasinski, and F. P. Zamborini (2012). *ACS Catal.* **2**, 2602.
31. G. J. Hutchings (2010). *Nat. Chem.* **2**, 1005.
32. J. Mao, Y. Liu, Z. Chen, D. Wang, and Y. Li (2014). *Bimet. Chem. Commun.* **50**, 4588.
33. S. E. Smith, A. R. Siamaki, B. F. Gupton, and E. E. Carpenter (2016). *RSC Adv.* **6**, 91541.
34. H. Sun, X. Jiao, H. Wang, Z. Jiang, and D. Chen (2011). *ACS Appl. Mater. Interfaces* **3**, 2425.
35. S. Ye, A. R. Rathmell, Z. Chen, I. E. Stewart, and B. J. Wiley (2014). *Adv. Mater.* **26**, 6670.
36. M. Mohl, P. Pusztai, A. Kukovecz, Z. Konya, J. Kukkola, K. Kordas, R. Vajtai, and P. M. Ajayan (2010). *Langmuir* **26**, 16496.
37. E. Koposova, A. Kisner, G. Shumilova, Y. Ermolenko, A. Offenhausser, and Y. Mourzina (2013). *J. Phys. Chem. C* **117**, 13944.
38. M. S. Bakshi (2016). *Cryst. Growth Des.* **16**, 1104.
39. V. R. Choudhary, B. Prabhakar, A. M. Rajput, and A. S. Mamman (1998). *Fuel* **77**, 1477.
40. Z. Li, J. Gao, X. Xing, S. Wu, S. Shuang, C. Dong, M. C. Paau, and M. M. F. Choi (2010). *J. Phys. Chem. C* **114**, 723.
41. G. Cao *Nanostructures & Nanomaterials: Synthesis, Properties & Applications* (Imperial College Press, London, 2004).
42. H. Sun, X. Jiao, H. Wang, Z. Jiang, and D. Chen (2011). *ACS Appl. Mater. Interfaces* **3**, 2425.

43. S. Nath, S. Praharaj, S. Panigrahi, S. Kundu, S. K. Ghosh, S. Basu, and T. Pal (2006). *Colloids Surf. A* **274**, 145.
44. X. Hou, X. Zhang, Y. Fang, S. Chen, N. Li, and Q. Zhou (2011). *J. Nanopart. Res.* **13**, 1929.
45. C. M. Shen, Y. K. Su, H. T. Yang, T. Z. Yang, and H. J. Gao (2003). *Chem. Phys. Lett.* **373**, 39.
46. Z. Chen, B. H. Loo, Y. Ma, Y. Cao, A. Ibrahim, and J. Yao (2004). *ChemPhysChem* **5**, 1020.
47. S. Gu, Y. Lu, J. Kaiser, M. Albrecht, and M. Ballauff (2015). *Phys. Chem. Chem. Phys.* **17**, 28137.
48. V. S. Suvith and D. Philip (2014). *Spectrochim. Acta A* **118**, 526.
49. L. Q. Zheng, X. D. Yu, J. J. Xu, and H. Y. Chen (2015). *Chem. Commun.* **51**, 1050.